Monthly Notices of the ROYAL ASTRONOMICAL SOCIETY
MNRAS **528,** 3186–3197 (2024) https://doi.org/10.1093/mnras/stae188

Characterizing HOD in filaments and nodes of the cosmic web

Noelia R. Perez,[1]★ Luis A. Pereyra,[2,3]★ Georgina Coldwell [1], Facundo Rodriguez [2,3] Ignacio G. Alfaro[2,3] and Andrés N. Ruiz [2,3]

[1]*Facultad de Ciencias Exactas, Físicas y Naturales, Departamento de Geofísica y Astronomía, CONICET Universidad Nacional de San Juan, Av. Ignacio de la Roza 590 (O), J5402DCS Rivadavia, San Juan, Argentina*
[2]*Instituto de Astronomía Teórica y Experimental, CONICET-UNC, Laprida 854, X5000BGR Córdoba, Argentina*
[3]*Observatorio Astronómico de Córdoba, UNC, Laprida 854, X5000BGR Córdoba, Argentina*

Accepted 2024 January 12. Received 2023 December 21; in original form 2023 July 7

ABSTRACT

The standard paradigm for the formation of the Universe suggests that large structures are formed from hierarchical clustering by the continuous accretion of less massive galaxy systems through filaments. In this context, filamentary structures play an important role in the properties and evolution of galaxies by connecting high-density regions, such as nodes, and being surrounded by low-density regions, such as cosmic voids. The availability of the filament and critical point catalogues extracted by DISPERSE from the ILLUSTRIS TNG300-1 hydrodynamic simulation allows a detailed analysis of these structures. The halo occupation distribution (HOD) is a powerful tool for linking galaxies and dark matter haloes, allowing constrained models of galaxy formation and evolution. In this work, we combine the advantage of halo occupancy with information from the filament network to analyse the HOD in filaments and nodes. In our study, we distinguish the inner regions of cosmic filaments and nodes from their surroundings. The results show that the filamentary structures have a similar trend to the total galaxy sample covering a wide range of densities. In the case of the nodes sample, an excess of faint and blue galaxies is found for the low-mass haloes suggesting that these structures are not virialized and that galaxies may be continuously falling through the filaments. Instead, the higher mass haloes could be in a more advanced stage of evolution showing features of virialized structures.

Key words: methods: statistical – galaxies: haloes – galaxies: statistics – large-scale structure of Universe.

1 INTRODUCTION

In the current Standard Model of Cosmology, Λ Cold Dark Matter (ΛCDM) baryons and dark matter accounts roughly 30 per cent of the total energy-matter, which are arranged in a complex and massive network known as the 'Cosmic Web' (de Lapparent, Geller & Huchra 1986; Bond, Kofman & Pogosyan 1996). The web pattern is composed of nodes, filaments and voids, and its study allows us to understand the evolutionary process of the Universe.

Filaments are traced by galaxies and transport matter from voids and walls to nodes (Zel'dovich 1970; Cautun et al. 2014). Nodes are typically found in regions of high density and voids inhabit regions of significantly lower density. As for to filaments, they span a wide range of densities, from superdense regions (though lower than nodes) to subdense regions (though higher than voids). The density threshold is therefore not sufficient to characterize a particular cosmic environment (Cautun et al. 2014).

In this context, Shandarin & Zeldovich (1989) suggest that dark matter haloes are formed from initial density perturbations in the density field of the early Universe and grow with time due to gravitational instability (Lifshitz 1946; Peebles 1980). Later, when these perturbations are dissociated from the expansion, they collapse into dark matter haloes, which continue to accrete material through hierarchical clustering by continuously merging smaller structures (White & Rees 1978; White 1994).

The galaxy formation and evolution are influenced by the environment, so it is expected that the large-scale surrounding affects their properties. Several works reveal the impact of these structures on galaxy shape and spin alignment (Faltenbacher et al. 2002; Trujillo, Carretero & Patiri 2006; Aragón-Calvo et al. 2007; Tempel & Libeskind 2013; Tempel, Stoica & Saar 2013; Forero-Romero, Contreras & Padilla 2014; Zhang et al. 2015; Ganeshaiah Veena et al. 2018, 2019; Wang et al. 2020; Lee & Moon 2023), and on properties such as galaxy stellar masses, star formation rate (SFR), and colour (Weinmann et al. 2006; Einasto et al. 2008; Lietzen et al. 2012; Darvish et al. 2016; Malavasi et al. 2017; Kraljic et al. 2018; Laigle et al. 2018).

The formation and evolution of galaxies in dark matter haloes depend on a variety of physical processes, and also because their properties are related to the host halo features. In this respect, it is not possible to determine exactly how galaxies populate the dark matter haloes in which they reside. The halo occupation distribution (HOD) model empirically links galaxies and dark matter haloes, characterizing the probability distribution $P(N|M)$ that a virialized halo of mass M contains N galaxies of previously determined characteristics (Peacock & Smith 2000; Berlind & Weinberg 2002; Berlind et al. 2003; Zheng et al. 2005; Guo et al. 2015; Rodriguez,

★ E-mail: noeliarocioperez@gmail.com (NP); luis.pereyra@unc.edu.ar (LP)

Merchán & Sgró 2015; Rodriguez & Merchán 2020). Moreover, Peacock & Smith (2000) argued that the distribution of galaxies within the halo density field depends on their position and the number of objects within the host halo. In this sense, the HOD formulation assumes that the host halo mass is the leading property that influences the galaxy properties (White & Rees 1978), although the spatial distribution of galaxies also depends on other properties (formation time, spin, concentration, neighbour mass, large-scale structure), known as the assembly bias (Gao, Springel & White 2005; Gao & White 2007; Mao, Zentner & Wechsler 2018; Musso et al. 2018; Salcedo et al. 2018; Ramakrishnan et al. 2019; Mansfield & Kravtsov 2020).

The HOD framework has been useful in constraining models of galaxy formation and evolution (Berlind et al. 2003; Kravtsov et al. 2004; Zehavi et al. 2018), and cosmological models (van den Bosch, Yang & Mo 2003; Zheng & Weinberg 2007) throughout the study of the dependence of the galaxy population properties (Berlind et al. 2003; Zheng et al. 2005; Contreras et al. 2013; Borzyszkowski et al. 2017; Zehavi et al. 2018; Yuan et al. 2022), and clustering variations with respect to large-scale environments (Artale et al. 2018; Zehavi et al. 2018; Alfaro et al. 2020; Alfaro et al. 2021; Alfaro et al. 2022). Furthermore, by characterizing the evolution of the clustering (Contreras & Zehavi 2023), interpreting the clustering data (Kim et al. 2009; Ross, Percival & Brunner 2010; Zehavi et al. 2011) and creating mock catalogues (Grieb et al. 2016) the halo population can be better understood.

We stress that our aim in this paper is to identify any differences that may exist for HODs in different cosmic web structures, taking into account a wide range of magnitude thresholds. We are also exploring the HOD considering different galaxy properties such as colour and morphology, in order to provide a comprehensive characterization. This paper is structured as follows: in Section 2 we summarize the data and describe the criteria for selecting samples. In Section 3 we analyse the HOD variations in nodes and filamentary structures, and their respective outskirts considering different magnitude limits. In this section, we also explore and compare the HOD for these environments with their surroundings taking into account diverse galaxy properties. Finally, in Section 4 we summarize and discuss the main results.

2 DATA

2.1 IllustrisTNG

This analysis has been based on the ILLUSTRISTNGproject[1] (Marinacci et al. 2018; Naiman et al. 2018; Nelson et al. 2018; Pillepich et al. 2018a,b; Springel et al. 2018), a suite of cosmological hydrodynamic simulations developed from the original ILLUSTRIS simulations (Genel et al. 2014; Vogelsberger et al. 2014a,b) and executed with the AREPO moving mesh code (Springel 2010). The cosmological parameters are in agreement with Planck 2015 results (Planck Collaboration XIII 2016): $\Omega_{\mathrm{m},0} = 0.3089$, $\Omega_{\Lambda,0} = 0.6911$, $\Omega_{\mathrm{b},0} = 0.0486$, $h = 0.6774$, $n_{\mathrm{s}} = 0.9667$, and $\sigma_8 = 0.8159$. The project has three sizes of physical simulation boxes, each with a side length of approximately 50, 100, and 300 Mpc, named TNG50, TNG100, and TNG300, respectively.

In particular, we used TNG300-1 because its higher resolution makes it the most suitable simulation for studying large-scale structures. TNG300-1 employs 2500^3 dark matter particles and 2500^3 gas particles with masses of $5.9 \times 10^7 \mathrm{M}_\odot$ and $1.1 \times 10^7 \mathrm{M}_\odot$, respectively, in a box of $205\,h^{-1}$Mpc. There are 100 snapshots available and each one is associated with a group catalogue containing haloes and subhaloes. Haloes (also named FoF Halo, FoF Group, or Group) are found using the friend-of-friend algorithm (Huchra & Geller 1982) with linking length $b = 0.2$ and the SUBFIND algorithm (Springel et al. 2001) is used to identify subhaloes (also known as Subfind Group, Subgroup, or Galaxies)

2.2 DisPerSE

The discrete persistent structures extractor, DISPERSE[2] (Sousbie 2011, 2013; Sousbie, Pichon & Kawahara 2011) is a multiscale identifier of structures based on discrete Morse theory. According to this theory, the Cosmic Web can be characterized in a mathematical equivalent called the Morse complex.

Initially, the algorithm generates the density field of a discrete set of points through the Delaunay tessellation field estimator (DTFE; Schaap & van de Weygaert 2000; van de Weygaert & Schaap 2009). This allows the identification of critical points, i.e. points where the density gradient is zero (maxima, minima, and saddle points). Then, Morse's theory uses mathematical properties that describe the relationship between topology and the geometry of the density field. The critical points together with their ascending and descending manifolds 0, 1, 2, and 3 can be related to clusters, filaments, walls, and voids, respectively. To quantify the importance of the topological features found, the user can select the persistence level for filtering the Poisson sample noise and intrinsic uncertainty within the data set.

For this work, we use the filaments and critical point catalogues developed by Duckworth, Tojeiro & Kraljic (2020a) and Duckworth et al. (2020b)[3] using the DISPERSE code, and available for TNG300-1. To build these catalogues, the authors selected subhaloes with masses higher than $M_* > 10^{8.5}\,h^{-1}\,\mathrm{M}_\odot$ and set the persistence parameter $\sigma = 4$ to remove spurious filaments. The catalogues are available for eight snapshots between $z = 0$ and $z = 2$ and provide the cosmic web distances between each subhalo to the nearest minimum critical point, the nearest 1-saddle point, the nearest 2-saddle point, the nearest maximum critical point, and the nearest filament segment (see for instance Duckworth, Tojeiro & Kraljic 2020a).

2.3 Sample selection

The sample used in this paper was constructed from the TNG300-1 Groupcat at $z = 0$ by selecting subhaloes with $M_* > 10^{8.5}\,h^{-1}\mathrm{M}_\odot$, in agreement with the filament catalogue, contained in haloes with masses $M_{200} \geq 10^{11}\,h^{-1}\mathrm{M}_\odot$, where M_{200} is the mass enclosed within a region that encompasses 200 times the critical density. The purpose of this selection is to obtain well-resolved haloes with about 10^3 particles. The final catalogue contained 212 749 haloes and 264 407 subhaloes.

With the aim of determining any existing differences in the halo occupation with respect to a variety of cosmic environments, we have separated the haloes according to whether they belong to regions such as nodes and filaments, respectively.

In the following, we will refer to nodes as haloes with a distance to maxima (peaks of the DisPerSE density field) less than R_{200} ($d_{\mathrm{n}} \leq 1R_{200}$), where R_{200} is the comoving radius of a sphere centred on

[1] https://www.tng-project.org/

[2] http://www2.iap.fr/users/sousbie/web/html/index888d.html?archive

[3] https://github.com/illustristng/disperse_TNG

Table 1. Percentage of haloes and subhaloes in each sample.

	Filaments (per cent)	Nodes (per cent)	Filament outskirts (per cent)	Node outskirts (per cent)	Unclassified (per cent)
Haloes	29.57	3.31	20.46	3.79	42.87
Subhaloes	29.23	30.71	13.32	2.81	23.93

the halo whose mean density is 200 times the critical density of the Universe. Meanwhile, for the filaments sample, we selected haloes with distance to the node $d_n > 1R_{200}$ and distance to the filament axis $d_f \leq 1h^{-1}$Mpc. This value was chosen to ensure that the objects belong to the filament core (Galárraga-Espinosa, Langer & Aghanim 2022; Galárraga-Espinosa, Garaldi & Kauffmann 2023).

To associate each halo and subhalo with a certain environment, we determined the distances from these objects to the nearest node and filament axis. Table 1 summarizes the percentage of haloes and subhaloes for each defined sample. The outskirt sample definitions are described in Sections 3.1 and 3.2. In addition, we show the percentages of halos and subhaloes not selected as part of our definitions in this work (Unclassified). We can observe that approximately half of the haloes are found in filament environments (filaments and filament outskirts), less than 10 per cent of the haloes inhabit node regions (nodes and node outskirts) and the rest are found in structures not considered in this work. This result is in agreement with Cautun et al. (2014) and Ganeshaiah Veena et al. (2019), who found that the dark matter fraction is contained in filaments, walls, voids, and nodes with 50, 25, 15, and 10 per cent, respectively. Although in the mentioned works, the fractions are calculated using the particles and not from the haloes.

3 ANALYSIS

The HOD allows us to statistically determine how many galaxies inhabit haloes with a mass within a given range (Berlind & Weinberg 2002). In this line, Alfaro et al. (2020) studied the HOD for central and satellite galaxies in very low-density environments, given by cosmic voids. They found a significant dependence of the halo occupation behaviour with the mass and luminosity of the galaxies. In addition, Alfaro et al. (2021) studied the HOD in a set of future virialized superstructures (FVS; Luparello et al. 2011) identified on a cosmological semi-analytic simulation to analyse the occupation of galaxies in haloes within globally high-density regions. The authors found that the HOD from high-mass haloes significantly increases towards the central regions of these superstructures.

In this section, we describe the procedure for the measurement of the HOD in different cosmic web structures, from the samples selected from the catalogues of the filament and point critics (Duckworth, Tojeiro & Kraljic 2020a; Duckworth et al. 2020b) as described in the previous section, and explore its dependence on several galaxy properties. To estimate the HOD, we compute the mean number of galaxies per halo mass bins, $<N_{gal}|M_{halo}>$, considering different ranges of r-band absolute magnitude for the subhalo. The error bars were determined using the jackknife technique (Quenouille 1949; Tukey 1958).

Following Alfaro et al. (2020), we use different absolute magnitude limits to compare the behaviour of faint and bright galaxies in the HOD. We selected the r-band because it is an estimator of stellar mass and could be compared with the observational data. The magnitude values used correspond to SubhaloStellarPhotometrics catalogue (Nelson et al. 2018). In Fig. 1, the HODs are shown for the total, nodes, and filaments samples considering the following r-magnitude thresholds: $M_r - 5\log_{10}(h) \leq -17, -18, -19$, and -20. The lower subpanels show the quotient between the nodes and filaments samples with respect to total HOD. As expected, the halo occupancy decreases when we consider increasingly brighter subhaloes. The HOD for haloes belonging to filaments is quite similar to that shown for the total sample, independent of galaxy luminosity. An increase in error can be observed for haloes with masses higher than $10^{14.5}\,h^{-1}\mathrm{M}_\odot$.

On the other hand, for the nodes sample, there is a significant excess of faint galaxies compared to the filaments and total samples. The main difference in the HOD between the samples occurs for haloes with masses lower than $10^{13}\,h^{-1}\mathrm{M}_\odot$, where we see that the HOD measured for the nodes is approximately two times higher than that measured for the filaments for the magnitude limit: $M_r - 5\log_{10}(h) \leq -17$. This discrepancy decreases and becomes imperceptible as we look at brighter galaxies, so this dependence on the magnitude thresholds could be related to the presence of satellite galaxies in the lower mass haloes. The distributions for haloes with masses $M_{halo} > 10^{13}\,h^{-1}\mathrm{M}_\odot$ are comparable. The error bars in the extreme regions, especially for the filaments sample, is related to the fact that there are few massive haloes in these structures, so the last bins are almost free of objects.

The study conducted by Alfaro et al. (2021) in high-density regions (FVS) reveals a different trend compared to the nodes examined in this work. In particular, the FVS showed an increase in the mean number of galaxies in haloes with masses greater than $\sim 10^{13}h^{-1}\mathrm{M}_\odot$, regardless of their luminosity, whereas no significant deviations were observed in the nodes compared to the whole halo sample. On the contrary, for halo masses smaller than about $10^{13}h^{-1}\mathrm{M}_\odot$, the HOD within the FVS shows negligible fluctuations. Instead, the HODs of nodes demonstrate significant differences in low-mass haloes, with a stronger luminosity dependence for the magnitude threshold of $M_r - 5\log_{10}(h) \leq -17$. Then, to enable a more comprehensive analysis within this luminosity range, we have set this limit, and also the limit corresponding to the brightest r-magnitude threshold, for analysis in the upcoming sections.

Since the differences detected in the HODs could be related to the properties of the galaxies, we performed an exhaustive analysis using galaxy colours since this property provides us with information on morphology, age, and evolution (Blanton et al. 2005; Vulcani et al. 2015). In Fig. 2, we plotted the galaxy colour distributions for filaments, nodes, and total samples considering the halo mass bins. In accordance with Nelson et al. (2018), the general tendency suggests that low-mass haloes are mainly populated by blue galaxies, with a small contribution from the red ones. Furthermore, as the haloes become more massive, the number of red galaxies increases while the number of blue galaxies gradually decreases. Finally, massive haloes are populated by red galaxies, suggesting the presence of a more evolved population. Regarding the nodes and filaments samples, for massive haloes, the galaxy colours in both samples are comparable to the total sample. As for the low-mass haloes, we found that the filaments sample follows the overall trend, whereas the nodes sample shows a remarkable bimodal colour distribution. This behaviour could be explained by the fact that the low-mass nodes represent local density maxima in the cosmic web inhabited by galaxies groups, which show evidence of physical processes that redden them even before they reach the virial radius (Blanton et al. 2003; Kraljic et al. 2018).

To complement the analysis, we determine the morphology using the supplementary catalogue of stellar circularities, angular momentum, and axis ratios (Genel et al. 2015). The morphology, together with colour and star-formation rate (SFR) allows us to characterize

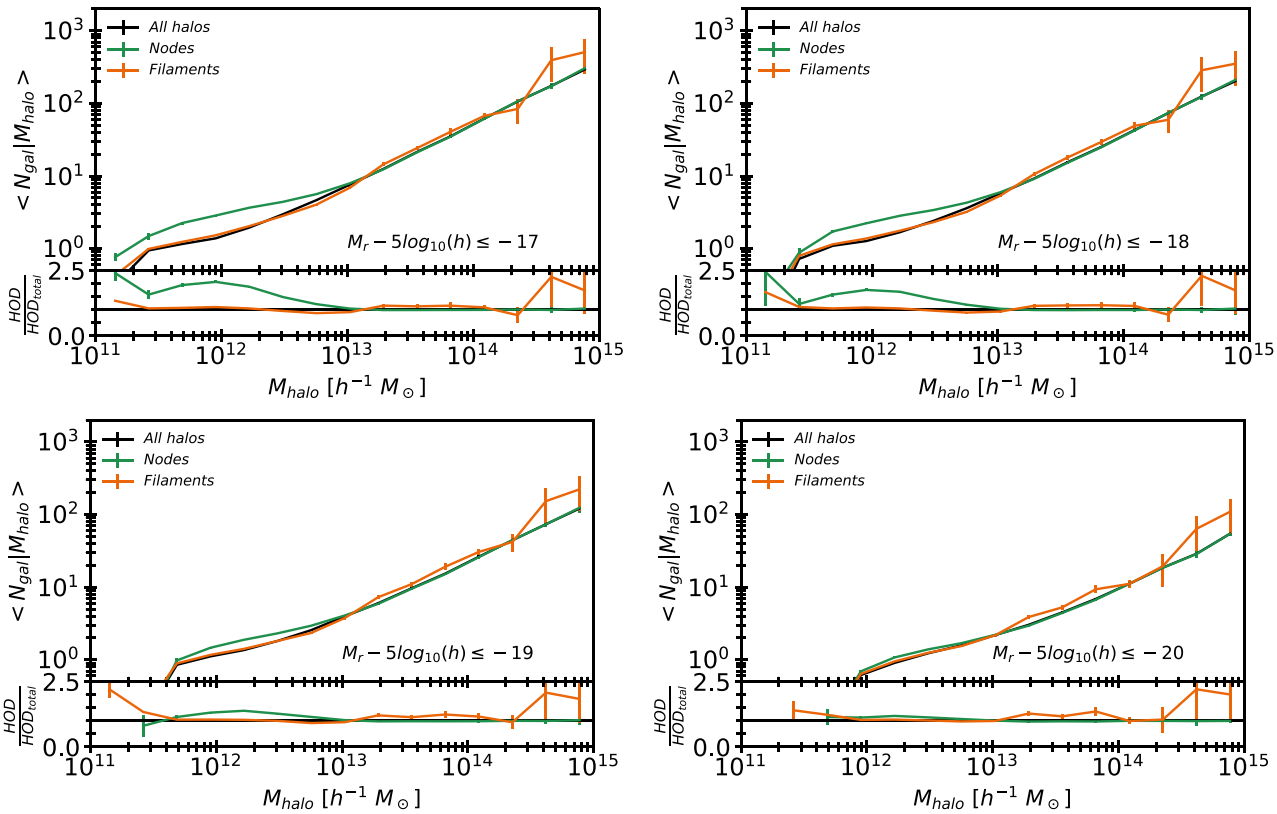

Figure 1. The panels show the HODs measured for galaxies with different magnitude thresholds for the whole sample and for galaxies belonging to filaments and node , respectively. Lower subpanels show the ratio between the HOD inside filaments and nodes and the HOD in the whole sample.

the galaxy properties within specific haloes. The correlation between these parameters indicates that late blue galaxies have a higher SFR than early red galaxies (e.g. Schawinski et al. 2014).

In order to calculate the HODs, we separate the subhaloes with respect to the parameters mentioned above. To exploit the bimodality of galaxy colours, we choose a value of $M_g - M_r = 0.6$ as the cut-off to distinguishing red ($M_g - M_r > 0.6$) from blue ($M_g - M_r \leq 0.6$) galaxies (Nelson et al. 2018). Then, to define discy (spheroidal) galaxies, we use the circularity parameter as a criterion, defining the bulge mass fraction as twice the stellar mass fraction with a negative circularity parameter lower (higher) than 0.5 (see e.g. Osato & Okumura 2023).

In the next subsections, we analyse the HODs for filaments, nodes, and their surrounding regions separately, in order to study both environments in more detail. For completeness, the Appendix presents the HODs acquired using the SFR parameter to distinguish between quiescent and star-forming galaxies.

3.1 Filaments

Taking into account the previous results, in this subsection we have focused on the analysis of the HOD in filamentary structures, considering the variations with respect to the distance to the filament axis. Then, we consider the filaments sample, which remains unchanged, and the filament outskirts sample defined by selecting haloes with $d_n > 1\,R_{200}$ to exclude the nodes and $1 < d_f\,[h^{-1}\mathrm{Mpc}] \leq 2$, considering an intermediate region between filaments and voids. The number of haloes and subhaloes in each sample is given in Table 1.

The HODs for filaments and filament outskirts are shown in Fig. 3. In upper panel we show the HOD for galaxies with $M_r - 5\log_{10}(h) \leq -17$. It can be observed that for halo masses smaller than $10^{12}\,h^{-1}\mathrm{M}_\odot$ the tendency of both samples is similar following the overall trend. This fact suggests that the process by which galaxies populate these haloes may be similar, regardless of the environment. For $M_{\mathrm{halo}} > 10^{12}\,h^{-1}\mathrm{M}_\odot$, the filaments and total HODs are indistinguishable within the error bars, while for the filament outskirts sample the curve is lower and corresponds to an environment without the presence of massive haloes. This result is in agreement with the trend found by Alfaro et al. (2020), who studied the HOD in environments with 10 per cent of the mean density of large scale tracers, reaching a halo mass of $\sim 10^{13}\,h^{-1}\mathrm{M}_\odot$, a similar mass range to the filament outskirts. Furthermore, they found that for haloes more massive than $10^{12}\,h^{-1}\mathrm{M}_\odot$, the HOD in voids it is up to 50 per cent lower than the overall trend. The lower panel of Fig. 3 shows the HOD taking into account only the brighter galaxies, i.e. galaxies with $M_r - 5\log_{10}(h) \leq -20$. For haloes with $M_{\mathrm{halo}} < 10^{13}\,h^{-1}\mathrm{M}_\odot$, the distributions of both samples overlaps the HOD corresponding to the total sample. Then, in the outskirts, the HOD shows a decrease, which is related to the small number of haloes in the mass range of $10^{13} < M_{\mathrm{halo}}[h^{-1}\mathrm{M}_\odot] < 10^{14}$. Respect to the filaments, the HOD covers the entire mass range and varies within the error bars with respect to the total sample. We found no significant differences when considering faint and bright galaxies separately. That is, the HODs for both filamentary environments show similar behaviour with respect to the magnitude of the galaxies considered. Then, for the subsequent analysis, we will investigate galaxies with $M_r - 5\log_{10}(h) \leq -17$, encompassing a more comprehensive range of magnitudes.

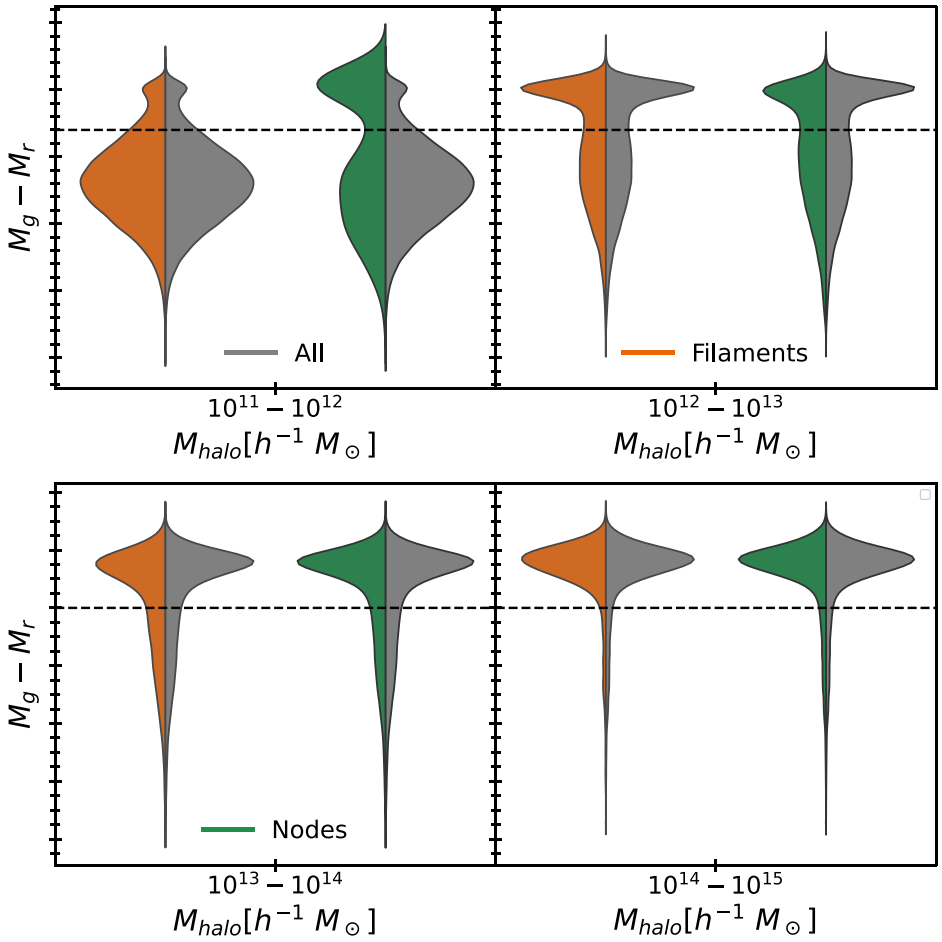

Figure 2. Galaxy colour distributions, in the halo mass bins, for the total sample, the filaments sample, and the nodes sample.

On the other hand, we explore the galaxy colour distributions, with respect to halo mass bins, for filaments and their outskirts samples. In Fig. 4, it can be seen that both environments have comparable distributions for $M_{\rm halo} < 10^{13}\,h^{-1}{\rm M}_\odot$. Also, for masses in the range $10^{13} < M_{\rm halo}\,[h^{-1}{\rm M}_\odot] < 10^{14}$, the samples suggest that the galaxies are predominantly red, although the distribution of the filament outskirts shows a higher dispersion with respect to the filament distribution. Furthermore, these surrounding regions do not have haloes with masses higher than $10^{14}\,h^{-1}{\rm M}_\odot$, as mentioned earlier.

Progressing with the analysis of HODs in terms of galaxy properties, in Fig. 5, we study the HODs for blue ($M_{\rm g} - M_{\rm r} \leq 0.6$) and red ($M_{\rm g} - M_{\rm r} > 0.6$) galaxies for each sample. As expected, the low-mass haloes are preferentially populated by blue galaxies, in contrast to the high-mass haloes dominated by red galaxies. The tendencies of the red galaxies for the two samples are close to each other and lie on the distribution of the total red galaxies. This suggests that the halo occupation by red galaxies is similar in both environments. On the other hand, an apparent disparity is observed when blue galaxies are considered. While the filaments sample tends to approximate the total blue sample within the error bars, the surrounding regions, corresponding to the filaments outskirts, show a slight decrease in blue galaxies as we consider more massive haloes.

The results of Kraljic et al. (2018) show that although the colour density segregation is milder in filaments than in regions of high peak density, it is still present, and it can be observed that red and passive galaxies are closer to the filaments than their star-forming and blue counterparts, regardless of the distance to the nodes. To understand the lack of blue galaxies in our filament outskirts for the intermediate halo masses, we examined the colour-density segregation for the defined blue and red galaxy samples considering three halo mass ranges, selected to visualize the colour-density tendencies in different halo mass ranges. In Fig. 6, the normalized distributions of blue and red galaxies in relation to the distance from the filament axis can be observed for low ($\rm M_{halo} \leq 10^{11.5}\,h^{-1}\,M_\odot$), intermediate ($\rm M_{halo} \in (10^{11.5}, 10^{12.5})\,h^{-1}\,M_\odot$), and high ($\rm M_{halo} > 10^{12.5}\,h^{-1}M_\odot$) mass range, respectively. For the low-mass halo region, close to the filament axis, the number of galaxies (both blue and red) decreases, making the morphological segregation unclear, while this effect becomes more pronounced towards the outer regions of the filament. Here, the proportion of blue galaxies increases with distance from the filament axis, in contrast to the proportion of red galaxies. For intermediate halo-masses, the colour-density segregation is still present but weaker. However, in the high halo-mass range, an excess of blue galaxies is observed close to the filament axis, and the trend is reversed. Then, the blue galaxies diminishing in high-mass haloes associated with the outskirts could be explained by most galaxies in these environments being reddened by local halo effects.

To conclude the analysis of the HOD taking into account the galaxy properties we show the distributions with respect to morphology, as described in previous section, in Fig. 7. The HODs for both filaments

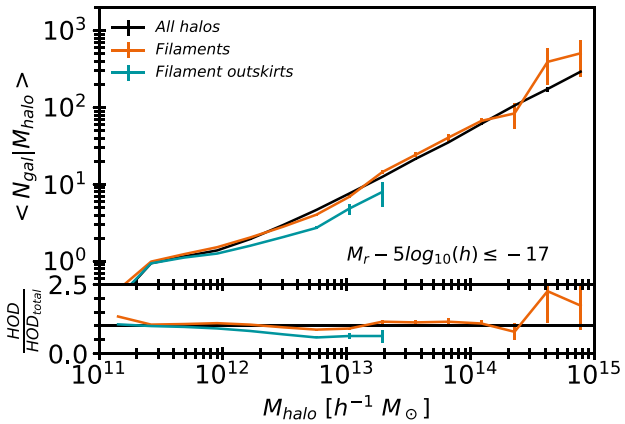

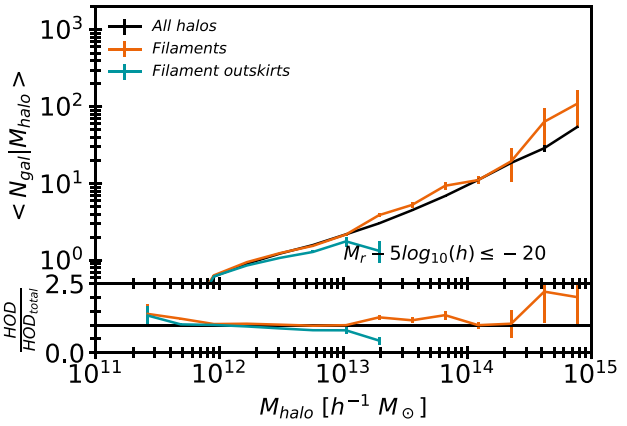

Figure 3. HODs measured for the total, filaments, and filament outskirts samples for subhaloes with $M_{\rm r} - 5{\rm log}_{10}({\rm h}) \leq -17$ (top panel) and $M_{\rm r} - 5{\rm log}_{10}({\rm h}) \leq -20$ (bottom panel), respectively. Sub-panels: the ratio between the filaments and filament outskirts samples respect to the overall HOD.

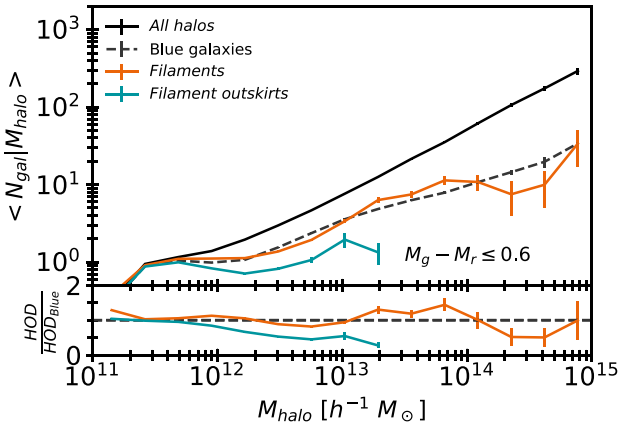

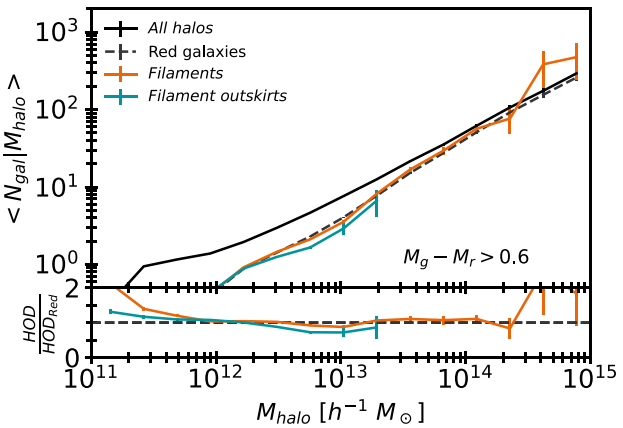

Figure 5. Panel shows the measured HOD with respect to the galaxy colours for the total, filaments, and filament outskirts samples for galaxies with $M_{\rm r} - 5{\rm log}_{10}({\rm h}) \leq -17$. The dashed lines represent the HODs for the total of blue (upper) and red (lower) galaxies. The lower sub-panels show the ratio of the filaments and filament outskirts samples to the total number of blue and red galaxies, respectively.

samples are comparable to the global trends, and although the HODs for filament outskirts are lower for both morphologies, the halo occupation is significantly lower for disc galaxies. These results are consistent with those obtained for galaxy colour.

The HODs measurements for the filaments sample, taking into account the studied galaxy properties, show that the halo occupancy in these environments is quite similar to the general trend, while haloes belonging to the filament outskirts show HODs up to 0.5 times lower than the general trend, despite the considered property. It is important to note that our definition of filament environment does not take into account the filament radius according to its density profile. Moreover, the results of this subsection suggest that the colour-density segregation is fulfilled for low-mass haloes (except for the regions close to the filamentary axis, where the number of galaxies is low and the result is therefore noisy), while decreasing for higher mass haloes, where the effect of local halo influences dominates over the proximity of the filamentary axis.

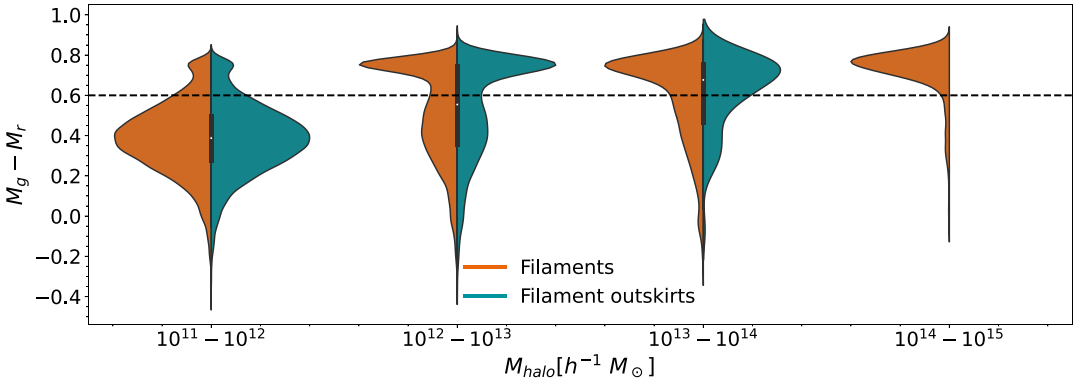

Figure 4. Colour distributions of galaxies in halo mass bins for filaments and filament outskirts samples.

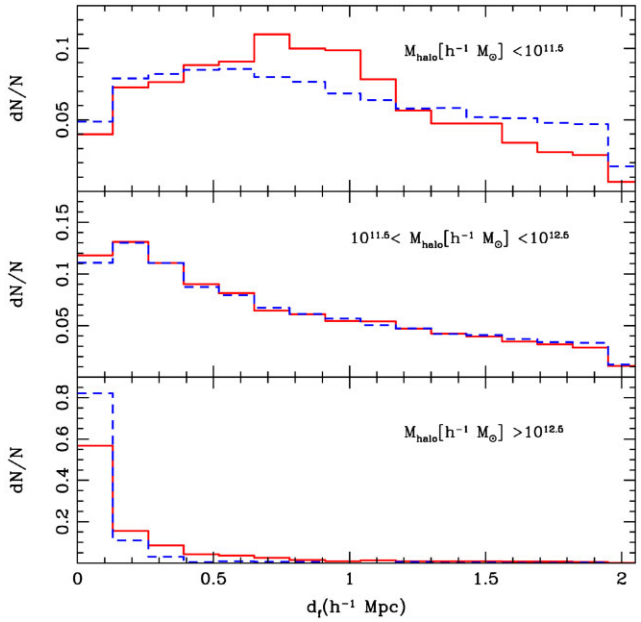

Figure 6. Normalized distributions of red and blue galaxies are presented for the low, intermediate, and high halo mass range in the top, middle, and bottom panels, respectively.

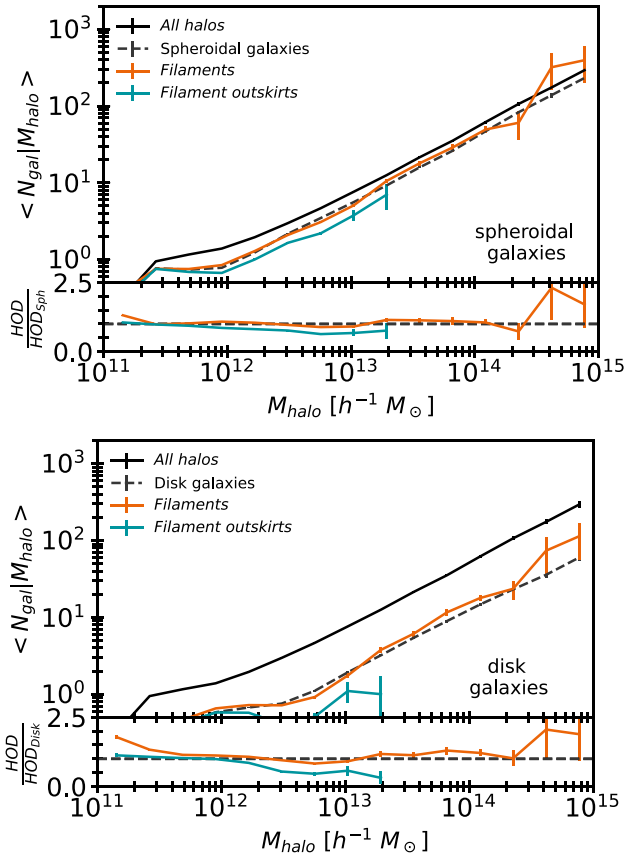

Figure 7. Panel shows the measured HOD with respect to the subhalo morphology for the total, filaments, and filament outskirts samples for subhaloes with $M_r - 5\log_{10}(h) \leq -17$. The dashed lines represent the HODs for the total of spheroidal (upper) and disc (lower) subhaloes. Lower subpanels show the ratio between the filaments and filament outskirts samples with the total of spheroidal and disc subhaloes, respectively.

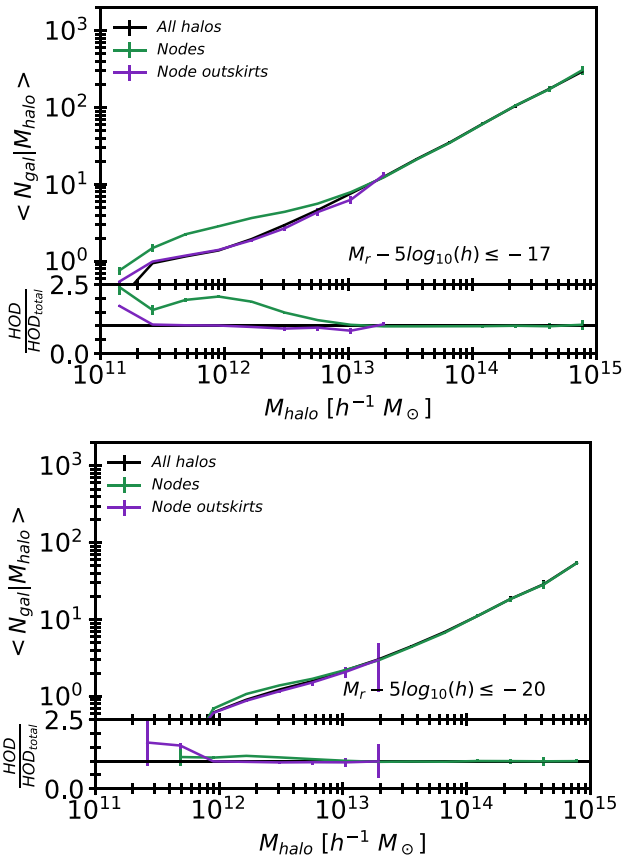

Figure 8. HODs measured for the total, nodes, and node outskirts samples for subhaloes with $M_r - 5\log_{10}(h) \leq -17$ (top panel) and $M_r - 5\log_{10}(h) \leq -20$ (bottom panel), respectively. Lower sub-panels show the ratio between the nodes and node outskirts samples with the overall HOD.

3.2 Nodes

For the sake of consistency, we apply the analysis of the previous subsection to the environments corresponding to the nodes sample. To account for HOD variations in the environment associated with such cosmic web structures, we have also constructed a sample of the node periphery, called node outskirts, by selecting haloes with $1 < d_n\,[R_{200}] \leq 3$ to obtain haloes in the node vicinity. The number of haloes and subhaloes can be found in Table 1.

In Fig. 8, we show the HODs for subhaloes, with magnitude threshold $M_r - 5\log_{10}(h) \leq -17$ and -20, for the total, nodes, and node outskirts samples. For the first magnitude threshold it is observed that the outskirts sample lies above the total sample, although in a smaller halo mass range due to the absence of massive haloes in these regions. That is, the node outskirts does not seem to have any influence on the halo occupancy. In addition, it can be observed that the behaviour within the range of masses covered is quite similar to that of the filament sample in the previous subsection. On the other hand, the node sample presents a remarkable difference for halo masses $M_{\rm halo} < 10^{13} h^{-1}{\rm M}_\odot$, where the HOD measured for the nodes is 2.5 times higher than the trend of the other samples. This result suggests an excess of faint galaxies in the low-mass halo population within nodes, indicating that the low-mass haloes are still in formation. Later forming haloes exhibit more recent accretion events, resulting in an excess of substructure. In contrast, early forming haloes contain fewer subhaloes due to more time for tidal

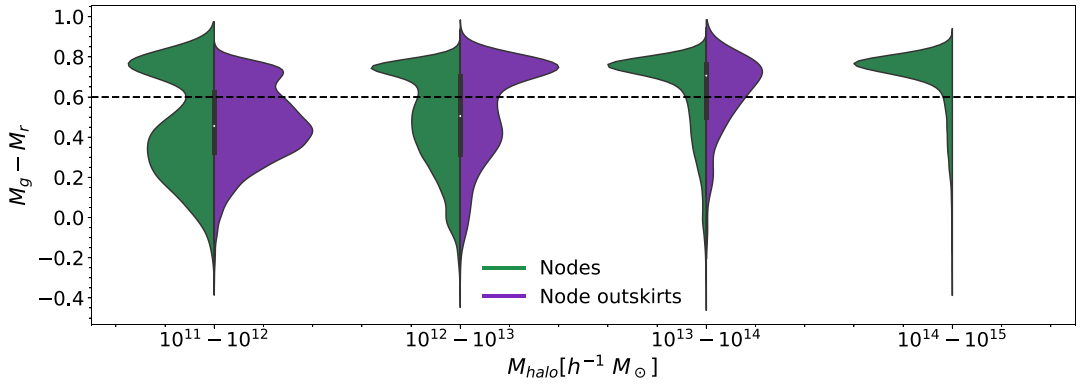

Figure 9. Galaxy colour distributions in halo mass bins for nodes and node outskirts samples.

disruption interactions or merging with the host halo via dynamical friction (Tinker et al. 2021).

Measuring the HOD using only the brightest galaxies, we find that the difference becomes negligible. Thus, the location of the host halo does not affect the occupation of the halo by a bright galaxy. As the largest difference in the measured HODs was detected at the magnitude threshold $M_r - 5\log_{10}(h) \leq -17$, we set this limit for the next analysis.

In line with the previous subsection, we examine the galaxy colour distributions for both environments in halo mass bins. Fig. 9 shows that low-mass haloes in nodes exhibit a distinct bimodal colour distribution, with the red component becoming more significant as mass increases, until the blue component disappears completely for massive haloes. This outcome is in line with galaxy colour change over time. In high-mass haloes in nodes, galaxies are more evolved as they have had more time to deplete their gas reserves and cease star formation, becoming redder. However, for the lower halo mass in nodes, many galaxies are still being accreted, leading to a population of young objects observed in the bimodal distribution. Nevertheless, the low-mass haloes within the node outskirts show a distinct colour bimodality with an overpopulation of objects in the green valley. Also, the red component becomes more significant with increasing mass. The last mass bin is empty, reflecting the reason for the mass limit in the HODs for these environments. These differences between galaxy colours at the nodes and at their periphery could be explained by environmental morphological segregation (Domínguez, Muriel & Lambas 2001). Then, the node outskirts allows us to find galaxies relatively uninfluenced by the dominant effects within the nodes. In addition, Martínez, Coenda & Muriel (2008) found that colour is the property that depends most on the distance from the centre of the cluster. In this sense, the overpopulation of galaxies in the green valley in haloes belonging to node outskirts sample could be related to the fact that the colour of these objects is affected by their proximity to the node.

Following the same line as the one in the previous subsection in Fig. 10, we show the HODs considering the galaxy colours. In the case of blue galaxies (upper panel), the nodes sample shows an excess of blue galaxies for haloes with masses lower than $10^{13}h^{-1}\mathrm{M}_\odot$ while the haloes inhabiting in the node outskirts exhibit a HOD slightly lower than the average HOD, within the error bars. For the red galaxies (lower panel), the trends for the HODs for both samples (nodes and their outskirts) are similar and lie close to the distribution of the total red galaxies. This result suggests that the occupation of the halo by blue galaxies depends on their location respect to the node centre, while red galaxies populate the haloes regardless of their environment.

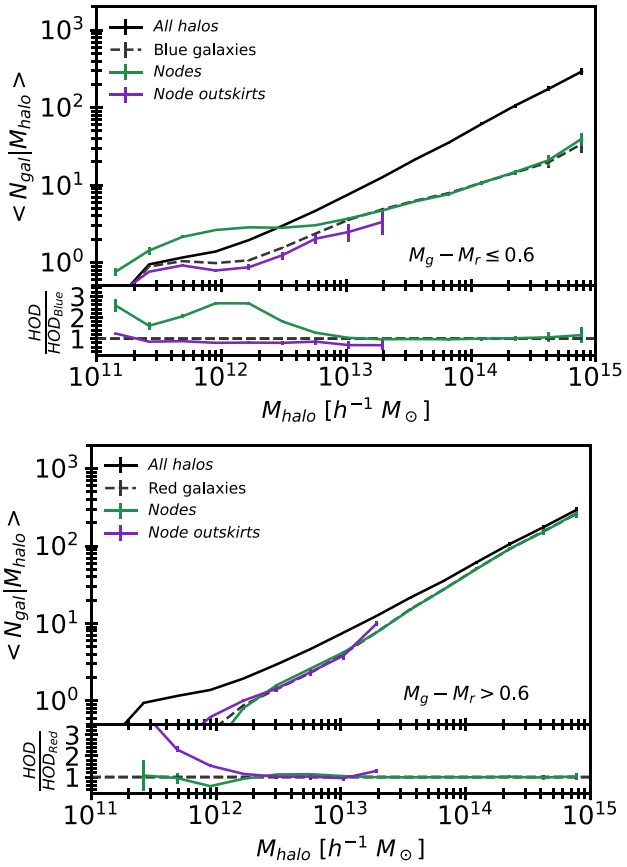

Figure 10. The main panel shows the measured HODs with respect to the galaxy colours for three samples: total, nodes, and node outskirts, considering the subhaloes with a magnitude of $M_r - 5\log_{10}(\mathrm{h}) \leq -17$. The dashed lines in the upper and bottom panels represent the HODs for the total blue and red galaxies, respectively. Bellow each panel, we plot the ratio of the nodes and node outskirts samples with respect to the total number of blue and red galaxies.

Finally, in Fig. 11 we show the HODs as a function of the galaxy morphology. The HODs calculated with spheroidal galaxies indicate that low-mass haloes in nodes have an excess of early-type galaxies with respect to the total sample. In the intermediate mass range, the distribution decreases until it overlaps with the HOD for a total of spheroidal galaxies. On the other hand, the node outskirts sample

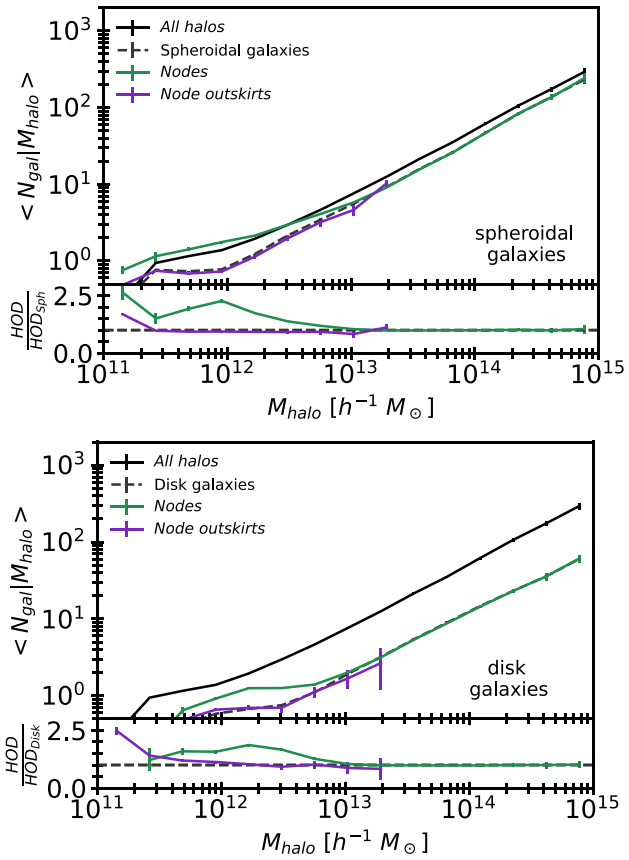

Figure 11. Panel shows the measured HODs with respect to the subhalo morphology for the total, nodes, and node outskirts samples for subhaloes with $M_r - 5\log_{10}(h) \leq -17$. The dashed lines represent the HODs for the total of spheroidal (upper) and disc (lower) subhaloes. Lower sub-panels show the ratio between the nodes and node outskirts samples with the total of spheroidal and disc subhaloes, respectively.

coincides with the total early-type galaxies distribution, regardless of halo mass. For disc galaxies, the HOD for node haloes is higher than the total distribution of disc galaxies in the low-mass region, but both samples overlap in the high-mass halo region. The HOD for haloes in the vicinity of nodes is close to the total distribution of disc galaxies, with a slight difference in the low-mass halo range. Galaxy accretion in these regions is likely to result in many interactions that affect galaxy morphology. However, the morphology of galaxies in low-mass haloes is not an entirely reliable parameter.

The HODs measured for the nodes sample show an excess of faint and blue galaxies for low-mass haloes. Regarding to the morphology, the HODs show an excess of spheroidal and disc galaxies in the lower mass range. These trends could be related to the measurement of the circularity parameter for low-mass galaxies, which have few stars to obtain an accurate result (Abadi et al. 2003). On the other hand, the halo occupancy in the node outskirts is quite similar to the overall trend, regardless of the property considered.

4 SUMMARY AND CONCLUSIONS

We have performed the HOD measurements for haloes derived from Groupcat at $z = 0.00$ from ILLUSTRIS TNG300-1 simulations. First, we separated haloes belonging to filaments and nodes, taking into account the distance to the node and to the filament axis. The nodes sample was constructed by considering haloes with distance to the node $d_n \leq 1\,R_{200}$ and for the filaments sample we selected haloes with distance to the node $d_n > 1\,R_{200}$ and distance to the filament axis $d_f \leq 1\,h^{-1}$Mpc.

We compute the mean number of galaxies per halo mass bin for the total, nodes, and filaments samples considering four magnitude thresholds: $M_r - 5\log_{10}(h) \leq -17, -18, -19$, and -20, following the line of Alfaro et al. (2020). We find that the HOD decreases when we consider increasingly brighter galaxies. Furthermore, the HOD for haloes in filaments is similar to that shown for the total sample, regardless of galaxy luminosity. This may suggest that the filamentary environment does not play a significant role in the occupancy of galaxies in haloes, since the halo mass of the host galaxy could be the primary factor influencing the properties of the galaxy, as suggested by White & Rees (1978). On the other hand, the nodes sample shows a significant excess of faint galaxies at lower halo masses, which decreases for bright galaxies. Low-mass haloes could have low rates of interaction and merging or may have undergone recent accretion processes. Therefore, these areas would favour the presence of faint galaxies. Since the differences in the HOD measurements are more pronounced for the $M_r - 5\log_{10}(h) \leq -17$ magnitude limit, we have chosen this cut-off magnitude for a more detailed analysis in the following.

The distribution of colours in the total sample indicates that galaxies in low-mass haloes are bluer. As mass increases, the galaxies become redder, which is consistent with the findings of Nelson et al. (2018). The filaments and nodes samples follow the general trend, except for low-mass haloes associated with nodes, which have a bimodal colour distribution. These low-mass nodes may represent local density maxima in the cosmic web that contain groups of galaxies. The bimodal distribution may indicate physical processes that cause galaxies to redden before they reach the virial radius (Blanton et al. 2003; Kraljic et al. 2018). Later, we measure the HODs taking into account several galaxy properties such as colour and morphology in filaments, nodes, and their surrounding regions.

Then, in order to study the variations associated with the distance to filamentary structures we define a filament outskirts sample by selecting haloes with $d_n > 1R_{200}$ and $1 < d_f\,[h^{-1}\text{Mpc}] \leq 2$. The HODs for subhaloes with $M_r - 5\log_{10}(h) \leq -17$ show that the filaments follow the overall trend, while the filament outskirts sample with $M_{halo} > 10^{12}\,h^{-1}\text{M}_\odot$ is 0.5 times lower than the total, suggesting that these less dense environments are less likely to be inhabited by galaxies. The HODs measured using the brighter galaxies show similar results, with both samples lying on the total HOD, despite the error bars. This result is in agreement with Alfaro et al. (2020), who found similar trends for even less dense regions such as cosmic voids. Looking at galaxy colours, despite the absence of the more massive haloes in the outskirts, the galaxy colour distributions are quite similar in both samples although, in the range of $10^{13} < M_{halo}[h^{-1}\text{M}_\odot] < 10^{14}$ the distribution of the filament outskirts shows a higher dispersion with respect to the filament distribution. The calculated HODs, discriminating the galaxy colours, show that the halo occupation of red galaxies is quite similar in both environments, while blue galaxies are less likely to be found in the outskirts than in the filaments for halo masses $M_{halo} > 10^{12}\,h^{-1}\text{M}_\odot$. In addition, the morphology analysis reveals that the haloes in the filaments are populated by disc and spheroidal galaxies, which is consistent with the overall trend. However, the outskirts of the filaments are generally devoid of galaxies, although they contain significantly fewer disc galaxies. To comprehend this outcome, we analyse the normalized distributions of blue and red galaxies with respect to the distance from the filament axis for different halo masses. We observed a pronounced

colour-density segregation, except near the filament axis, for $M_{\rm halo} < 10^{11.5}\,h^{-1}{\rm M}_{\odot}$, in agreement with Kraljic et al. (2018). As the halo mass increases, the degree of segregation weakens and for $M_{\rm halo} > 10^{12.5}\,h^{-1}{\rm M}_{\odot}$ the trend is reversed. The absence of blue galaxies in high-mass haloes situated in the filament outskirts may be attributed to a halo effect, such as the halo formation time (Tinker et al. 2021), or because the local dense environment has a greater influence on the galaxy properties (White & Rees 1978) than the global environment.

Following the study in the filamentary regions, we examined the nodes and their surrounding regions. The node outskirts sample was built considering haloes with $1 < d_{\rm n}\,[R_{200}] \leq 3$. Taking into account the magnitude limit $M_{\rm r} - 5{\rm log}_{10}(h) \leq -17$, we observe a remarkable excess of faint galaxies in the halo occupation for haloes with masses lower than $10^{13}h^{-1}{\rm M}_{\odot}$, while the outskirts follow the global trend. For galaxies with $M_{\rm r} - 5{\rm log}_{10}(h) \leq -20$, the HODs for both samples are similar to the total sample. The galaxy colour distributions for low-mass haloes are bimodal, and with increasing mass the red component becomes more significant in both samples, as stated by the environmental morphological segregation (Domínguez, Muriel & Lambas 2001), although there are no massive haloes in the outskirts. The HODs with respect to galaxy colours show an excess of blue galaxies for haloes with masses lower than $10^{13}\,h^{-1}{\rm M}_{\odot}$ in the nodes, while the node outskirts show a halo occupation slightly lower than the total sample. Regarding morphology, the HODs for nodes show an excess of both, disc and bulge galaxies, for nodes with masses lower than $10^{13}\,h^{-1}{\rm M}_{\odot}$, while the haloes within the node outskirts have an occupancy comparable to the global trend.

The halo occupation in filaments appears to be independent of the properties of the galaxies inhabiting these environments and similar to the global tendency. Instead of that the outskirts of the filaments show a lower halo occupancy. Regarding the nodes, the HODs for low-mass haloes show a significant difference with respect to the other samples. In this sense, the nodes could represent structures where the galaxies fall through the filaments, and they could be at different stages of evolution depending on their mass. These results could be related to the halo assembly bias, as proposed by Ramakrishnan et al. (2019) and Mansfield & Kravtsov (2020), who consider this important issue for the formation and evolution of the large structures of the Universe. Also, works such as Borzyszkowski et al. (2017) point out that such a bias is a product of the action of large structures in the Universe that cause the extinction of halo growth through tidal forces. In particular, they claim that 'stalled' haloes would be found at the nodes. The changes we observe in the HOD could result from just such a difference in the formation history of haloes.

The analysis carried out in this study provides insights into how galaxies populate the haloes, and how this depends on the mass of the halo and its position within the cosmic web. The study of the evolution of HODs leads to a very interesting topic of analysis, as suggested by Contreras & Zehavi (2023). In a forthcoming work, we will then assess the evolution of HODs in the large-scale environments given by nodes and filamentary structures.

ACKNOWLEDGEMENTS

We thank the referee, for providing us with helpful comments and suggestions that improved this paper. This work was supported in part by the Consejo Nacional de Investigaciones Científicas y Técnicas de la República Argentina (CONICET) and the Consejo Nacional de Investigaciones Científicas, Técnicas y de Creación Artística de la Universidad Nacional de San Juan (CICITCA). The authors would like to thank the ILLUSTRISTNG team for making their data available to the public. FR would like to acknowledge support from the ICTP through the Junior Associates Programme 2023–2028.

DATA AVAILABILITY

The simulation data underlying this article are publicly available at the TNG website. The data results arising from this work will be shared on reasonable request to the corresponding authors.

REFERENCES

Abadi M. G., Navarro J. F., Steinmetz M., Eke V. R., 2003, ApJ, 597, 21
Alfaro I. G., Rodriguez F., Ruiz A. N., Lambas D. G., 2020, A&A, 638, A60
Alfaro I. G., Ruiz A. N., Luparello H. E., Rodriguez F., Lambas D. G., 2021, A&A, 654, A62
Alfaro I. G., Rodriguez F., Ruiz A. N., Luparello H. E., Lambas D. G., 2022, A&A, 665, A44
Aragón-Calvo M. A., van de Weygaert R., Jones B. J. T., van der Hulst J. M., 2007, ApJ, 655, L5
Artale M. C., Zehavi I., Contreras S., Norberg P., 2018, MNRAS, 480, 3978
Berlind A. A., Weinberg D. H., 2002, ApJ, 575, 587
Berlind A. A. et al., 2003, ApJ, 593, 1
Blanton M. R. et al., 2003, ApJ, 594, 186
Blanton M. R., Eisenstein D., Hogg D. W., Schlegel D. J., Brinkmann J., 2005, ApJ, 629, 143
Bond J. R., Kofman L., Pogosyan D., 1996, Nature, 380, 603
Borzyszkowski M., Porciani C., Romano-Diaz E., Garaldi E., 2017, MNRAS, 469, 594
Cautun M., van de Weygaert R., Jones B. J. T., Frenk C. S., 2014, MNRAS, 441, 2923
Contreras S., Zehavi I., 2023, MNRAS, 525, 4257
Contreras S., Baugh C. M., Norberg P., Padilla N., 2013, MNRAS, 432, 2717
Darvish B., Mobasher B., Sobral D., Rettura A., Scoville N., Faisst A., Capak P., 2016, ApJ, 825, 113
de Lapparent V., Geller M. J., Huchra J. P., 1986, ApJ, 302, L1
Domínguez M., Muriel H., Lambas D. G., 2001, AJ, 121, 1266
Duckworth C., Tojeiro R., Kraljic K., 2020a, MNRAS, 492, 1869
Duckworth C., Starkenburg T. K., Genel S., Davis T. A., Habouzit M., Kraljic K., Tojeiro R., 2020b, MNRAS, 495, 4542
Einasto M. et al., 2008, ApJ, 685, 83
Faltenbacher A., Gottlöber S., Kerscher M., Müller V., 2002, A&A, 395, 1
Forero-Romero J. E., Contreras S., Padilla N., 2014, MNRAS, 443, 1090
Galárraga-Espinosa D., Langer M., Aghanim N., 2022, A&A, 661, A115
Galárraga-Espinosa D., Garaldi E., Kauffmann G., 2023, A&A, 671, A160
Ganeshaiah Veena P., Cautun M., van de Weygaert R., Tempel E., Jones B. J. T., Rieder S., Frenk C. S., 2018, MNRAS, 481, 414
Ganeshaiah Veena P., Cautun M., Tempel E., van de Weygaert R., Frenk C. S., 2019, MNRAS, 487, 1607
Gao L., White S. D. M., 2007, MNRAS, 377, L5
Gao L., Springel V., White S. D. M., 2005, MNRAS, 363, L66
Genel S. et al., 2014, MNRAS, 445, 175
Genel S., Fall S. M., Hernquist L., Vogelsberger M., Snyder G. F., Rodriguez-Gomez V., Sijacki D., Springel V., 2015, ApJ, 804, L40
Grieb J. N., Sánchez A. G., Salazar-Albornoz S., Dalla Vecchia C., 2016, MNRAS, 457, 1577
Guo H. et al., 2015, MNRAS, 453, 4368
Huang S. et al., 2019, MNRAS, 484, 2021
Huchra J. P., Geller M. J., 1982, ApJ, 257, 423
Kauffmann G., White S. D. M., Heckman T. M., Ménard B., Brinchmann J., Charlot S., Tremonti C., Brinkmann J., 2004, MNRAS, 353, 713
Kennicutt Robert C. J., 1998, ARA&A, 36, 189
Kennicutt R. C., Evans N. J., 2012, ARA&A, 50, 531
Kim H.-S., Baugh C. M., Cole S., Frenk C. S., Benson A. J., 2009, MNRAS, 400, 1527
Kraljic K. et al., 2018, MNRAS, 474, 547

Kravtsov A. V., Berlind A. A., Wechsler R. H., Klypin A. A., Gottlöber S., Allgood B., Primack J. R., 2004, ApJ, 609, 35
Laigle C. et al., 2018, MNRAS, 474, 5437
Lee J., Moon J.-S., 2023, ApJ, 951, L26
Lietzen H., Tempel E., Heinämäki P., Nurmi P., Einasto M., Saar E., 2012, A&A, 545, A104
Lifshitz E. M., 1946, Zh. Eksp. Teor. Fiz., 16, 587
Luparello H., Lares M., Lambas D. G., Padilla N., 2011, MNRAS, 415, 964
Malavasi N. et al., 2017, MNRAS, 465, 3817
Mansfield P., Kravtsov A. V., 2020, MNRAS, 493, 4763
Mao Y.-Y., Zentner A. R., Wechsler R. H., 2018, MNRAS, 474, 5143
Marinacci F. et al., 2018, MNRAS, 480, 5113
Martínez H. J., Coenda V., Muriel H., 2008, MNRAS, 391, 585
Moutard T., Sawicki M., Arnouts S., Golob A., Malavasi N., Adami C., Coupon J., Ilbert O., 2018, MNRAS, 479, 2147
Musso M., Cadiou C., Pichon C., Codis S., Kraljic K., Dubois Y., 2018, MNRAS, 476, 4877
Naiman J. P. et al., 2018, MNRAS, 477, 1206
Nelson D. et al., 2018, MNRAS, 475, 624
Osato K., Okumura T., 2023, MNRAS, 519, 1771
Peacock J. A., Smith R. E., 2000, MNRAS, 318, 1144
Peebles P. J. E., 1980, The Large-Scale Structure of the Universe. Princeton Univ. Press, Princeton
Peng Y.-j. et al., 2010, ApJ, 721, 193
Pillepich A. et al., 2018a, MNRAS, 473, 4077
Pillepich A. et al., 2018b, MNRAS, 475, 648
Pillepich A. et al., 2019, MNRAS, 490, 3196
Planck Collaboration XIII 2016, A&A, 594, A13
Quenouille M. H., 1949, Ann. Math. Stat., 20, 355
Ramakrishnan S., Paranjape A., Hahn O., Sheth R. K., 2019, MNRAS, 489, 2977
Rodriguez F., Merchán M., 2020, A&A, 636, A61
Rodriguez F., Merchán M., Sgró M. A., 2015, A&A, 580, A86
Ross A. J., Percival W. J., Brunner R. J., 2010, MNRAS, 407, 420
Salcedo A. N., Maller A. H., Berlind A. A., Sinha M., McBride C. K., Behroozi P. S., Wechsler R. H., Weinberg D. H., 2018, MNRAS, 475, 4411
Schaap W. E., van de Weygaert R., 2000, A&A, 363, L29
Schawinski K. et al., 2014, MNRAS, 440, 889
Shandarin S. F., Zeldovich Y. B., 1989, Rev. Mod. Phys., 61, 185
Sousbie T., 2011, MNRAS, 414, 350
Sousbie T., 2013, DisPerSE: Discrete Persistent Structures Extractor, Astrophysics Source Code Library, record ascl:1302.015
Sousbie T., Pichon C., Kawahara H., 2011, MNRAS, 414, 384
Springel V., 2010, MNRAS, 401, 791
Springel V., White S. D. M., Tormen G., Kauffmann G., 2001, MNRAS, 328, 726
Springel V. et al., 2018, MNRAS, 475, 676
Tempel E., Libeskind N. I., 2013, ApJ, 775, L42
Tempel E., Stoica R. S., Saar E., 2013, MNRAS, 428, 1827
Tinker J. L., Cao J., Alpaslan M., DeRose J., Mao Y.-Y., Wechsler R. H., 2021, MNRAS, 505, 5370
Trujillo I., Carretero C., Patiri S. G., 2006, ApJ, 640, L111
Tukey J. W., 1958, Ann. Math. Stat., 29, 614
Vogelsberger M. et al., 2014a, MNRAS, 444, 1518
Vogelsberger M. et al., 2014b, Nature, 509, 177
Vulcani B., Poggianti B. M., Fritz J., Fasano G., Moretti A., Calvi R., Paccagnella A., 2015, ApJ, 798, 52
Wang P., Libeskind N. I., Tempel E., Pawlowski M. S., Kang X., Guo Q., 2020, ApJ, 900, 129
Weinmann S. M., van den Bosch F. C., Yang X., Mo H. J., 2006, MNRAS, 366, 2
White S. D. M., 1994, Formation and Evolution of Galaxies: Les Houches Lectures, Astrophysics e-prints (arXiv:astro-ph/9410043)
White S. D. M., Rees M. J., 1978, MNRAS, 183, 341
Yuan S., Hadzhiyska B., Bose S., Eisenstein D. J., 2022, MNRAS, 512, 5793
Zehavi I. et al., 2011, ApJ, 736, 59
Zehavi I., Contreras S., Padilla N., Smith N. J., Baugh C. M., Norberg P., 2018, ApJ, 853, 84
Zel'dovich Y. B., 1970, A&A, 5, 84
Zhang Y., Yang X., Wang H., Wang L., Luo W., Mo H. J., van den Bosch F. C., 2015, ApJ, 798, 17
Zheng Z., Weinberg D. H., 2007, ApJ, 659, 1
Zheng Z. et al., 2005, ApJ, 633, 791
van de Weygaert R., Schaap W., 2009, in Martínez V. J., Saar E., Martínez-González E., Pons-Bordería M. J., eds, Data Analysis in Cosmology, Vol. 665. Springer, Heidelberg, p. 291
van den Bosch F. C., Yang X., Mo H. J., 2003, MNRAS, 340, 771

APPENDIX A: HOD MEASUREMENTS REGARDING TO THE SFR PARAMETER

The evolutionary history of galaxies can be inferred from the SFR parameter, which is related to the amount of gas and the efficiency of star formation (Kennicutt 1998). Several processes at scales between parsecs and Megaparsecs affect star formation (Kennicutt & Evans 2012), such as environment and galaxy mass (Kauffmann et al. 2004; Peng et al. 2010; Moutard et al. 2018). With this in mind, in order to complement the HODs measurements with respect to the galaxy properties of Section 3, we explore the SFR parameter. Following Pillepich et al. (2019), we calculate recursively star forming main sequence (SFMS) ridge line in the SFR versus stellar mass plane. Then, we define star-forming and quiescent galaxies as those above and below the SFMS line, respectively.

A1 Filaments

The HODs of quiescent and star-forming galaxies are shown in Fig. A1. Looking at the quiescent galaxies, we observe that the filaments sample lies on the total distribution of inactive galaxies. For high-mass haloes, the behaviour shows scattering caused by the low number of objects in these mass bins. The trend in the filament outskirts is comparable to that of the sample within the error bars. This implies that inactive galaxies do not display a preference for any of these environments. On the other hand, for low-mass haloes, we observe that the star-forming galaxies in the filaments sample have a HOD similar to the total of the star-forming galaxies, while for high-mass haloes the behaviours show a sinusoidal shape with respect to this distribution. Besides, haloes in the filament outskirts are practically devoid of star-forming galaxies. The results discovered at the periphery of the filament resemble those found in the void regions by Alfaro et al. (2020).

A2 Nodes

In addition, in Fig. A2 we show the HODs taking into account the SFR parameter. In the upper panel we observe the HODs for quiescent galaxies. The distributions of both samples lie on the HOD for total inactive subhaloes. This would mean that the occupancy by this type of galaxy is less dependent on specific environmental conditions. Finally, the lower panel shows the distributions for star-forming galaxies. Low-mass haloes in nodes have an excess of star-forming galaxies over the total active galaxies, which is even higher than the total feature, then for massive haloes the HOD decreases and is placed on the trend of the total star-forming galaxies. This may be related to the fact that the hot gas fraction decreases at low halo masses (Huang et al. 2019), favouring star formation in these haloes.

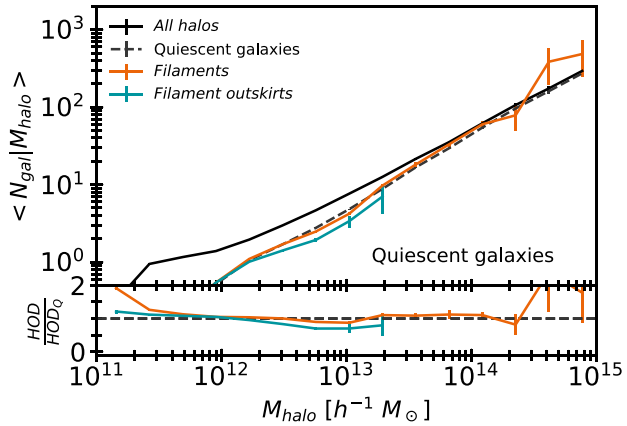

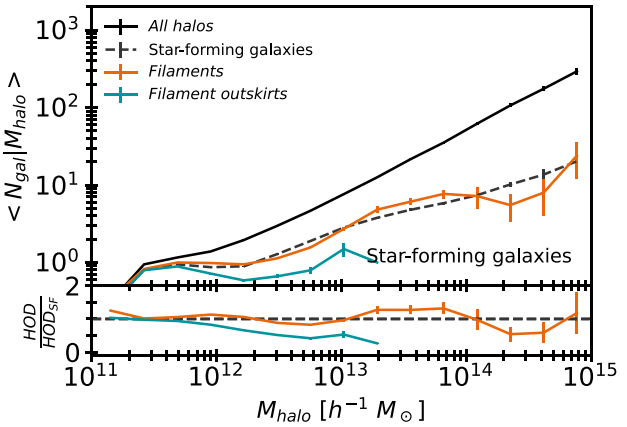

Figure A1. Panels shows the HODs measured with respect to the subhalo star formation rate parameter (SFR) for the total, filaments, and filament outskirts samples for subhaloes with $M_r - 5\log_{10}(h) \leq -17$. The dashed lines represent the HODs for the total of quiescent (upper) and star-forming (lower) subhaloes. Lower subpanels show the ratio between the filaments and filament outskirts samples with the total of quiescent and star-forming subhalos, respectively.

On the contrary, haloes in the regions surrounding the nodes have a lower distribution than the total active galaxy distribution for the whole range of masses.

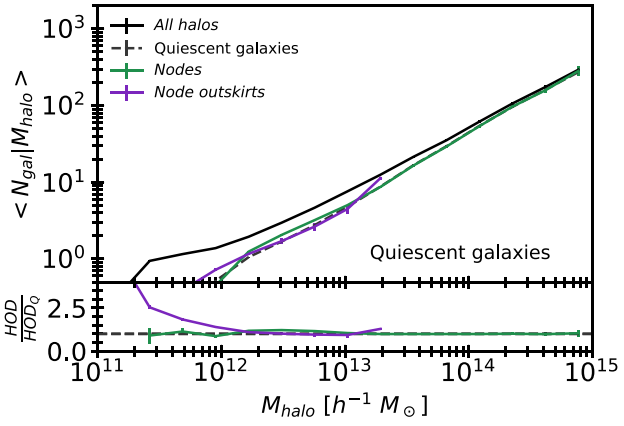

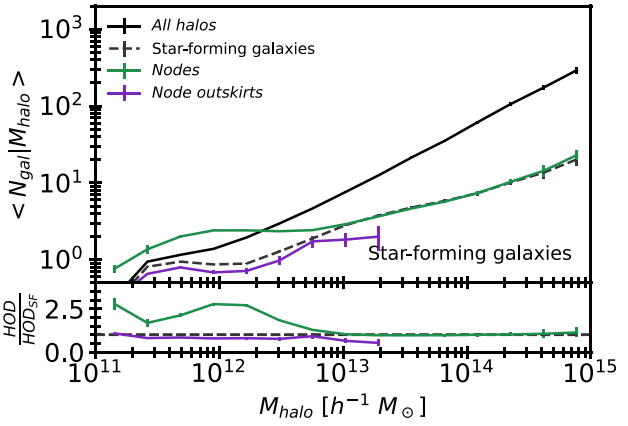

Figure A2. Panel shows the measured HOD with respect to the SFR parameter for the total, nodes, and node outskirts samples for subhaloes with $M_r - 5\log_{10}(h) \leq -17$. The dashed lines represent the HODs for the total of quiescent (upper) and star-forming (lower) subhaloes. Lower subpanels show the ratio between the nodes and node outskirts samples with the total of quiescent and star-forming subhalos, respectively.

This paper has been typeset from a TEX/LATEX file prepared by the author.